JOURNAL OF
Applied Polymer
SCIENCE

Special Issue: Polymers for Microelectronics

Guest Editors: Dr Brian Knapp (Promerus LLC) and
Prof. Paul A. Kohl (Georgia Institute of Technology)

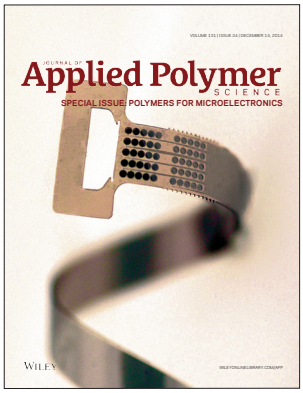

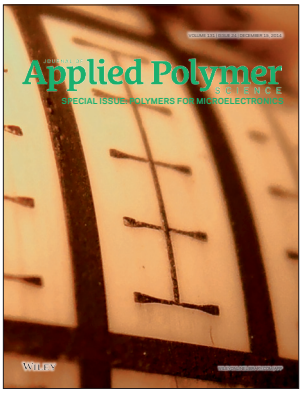

EDITORIAL

Polymers for Microelectronics
B. Knapp and P. A. Kohl, *J. Appl. Polym. Sci.* 2014, **DOI: 10.1002/app.41233**

REVIEW

Negative differential conductance materials for flexible electronics
A. Nogaret, *J. Appl. Polym. Sci.* 2014, **DOI: 10.1002/app.40169**

RESEARCH ARTICLES

Generic roll-to-roll compatible method for insolubilizing and stabilizing conjugated active layers based on low energy electron irradiation
M. Helgesen, J. E. Carlé, J. Helt-Hansen, A. Miller, and F. C. Krebs, *J. Appl. Polym. Sci.* 2014, **DOI: 10.1002/app.40795**

Selective etching of polylactic acid in poly(styrene)-block-poly(D,L)lactide diblock copolymer for nanoscale patterning
C. Cummins, P. Mokarian-Tabari, J. D. Holmes, and M. A. Morris, *J. Appl. Polym. Sci.* 2014, **DOI: 10.1002/app.40798**

Preparation and dielectric behavior of polyvinylidene fluoride composite filled with modified graphite nanoplatelet
P. Xie, Y. Li, and J. Qiu, *J. Appl. Polym. Sci.* 2014, **DOI: 10.1002/app.40229**

Design of a nanostructured electromagnetic polyaniline–Keggin iron–clay composite modified electrochemical sensor for the nanomolar detection of ascorbic acid
R. V. Lilly, S. J. Devaki, R. K. Narayanan, and N. K. Sadanandhan, *J. Appl. Polym. Sci.* 2014, **DOI: 10.1002/app.40936**

Synthesis and characterization of novel phosphorous-silicone-nitrogen flame retardant and evaluation of its flame retardancy for epoxy thermosets
Z.-S. Li, J.-G. Liu, T. Song, D.-X. Shen, and S.-Y. Yang, *J. Appl. Polym. Sci.* 2014, **DOI: 10.1002/app.40412**

Electrical percolation behavior and electromagnetic shielding effectiveness of polyimide nanocomposites filled with carbon nanofibers
L. Nayak, T. K. Chaki, and D. Khastgir, *J. Appl. Polym. Sci.* 2014, **DOI: 10.1002/app.40914**

Morphological influence of carbon modifiers on the electromagnetic shielding of their linear low density polyethylene composites
B. S. Villacorta and A. A. Ogale, *J. Appl. Polym. Sci.* 2014, **DOI: 10.1002/app.41055**

Electrical and EMI shielding characterization of multiwalled carbon nanotube/polystyrene composites
V. K. Sachdev, S. Bhattacharya, K. Patel, S. K. Sharma, N. C. Mehra, and R. P. Tandon, *J. Appl. Polym. Sci.* 2014, **DOI: 10.1002/app.40201**

Anomalous water absorption by microelectronic encapsulants due to hygrothermal-induced degradation
M. van Soestbergen and A. Mavinkurve, *J. Appl. Polym. Sci.* 2014, **DOI: 10.1002/app.41192**

Design of cyanate ester/azomethine/ZrO_2 nanocomposites high-k dielectric materials by single step sol-gel approach
M. Ariraman, R. Sasi Kumar and M. Alagar, *J. Appl. Polym. Sci.* 2014, **DOI: 10.1002/app.41097**

Furan/imide Diels–Alder polymers as dielectric materials
R. G. Lorenzini and G. A. Sotzing, *J. Appl. Polym. Sci.* 2014, **DOI: 10.1002/app.40179**

High dielectric constant polyimide derived from 5,5'-bis[(4-amino) phenoxy]-2,2'-bipyrimidine
X. Peng, Q. Wu, S. Jiang, M. Hanif, S. Chen, and H. Hou, *J. Appl. Polym. Sci.* 2014, **DOI: 10.1002/app.40828**

The influence of rigid and flexible monomers on the physical-chemical properties of polyimides
T. F. da Conceição and M. I. Felisberti, *J. Appl. Polym. Sci.* 2014, **DOI: 10.1002/app.40351**

JOURNAL OF
Applied Polymer
SCIENCE

Special Issue: Polymers for Microelectronics

Guest Editors: Dr Brian Knapp (Promerus LLC) and
Prof. Paul A. Kohl (Georgia Institute of Technology)

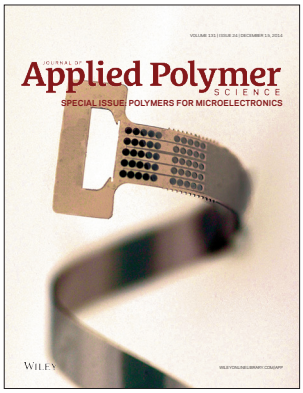

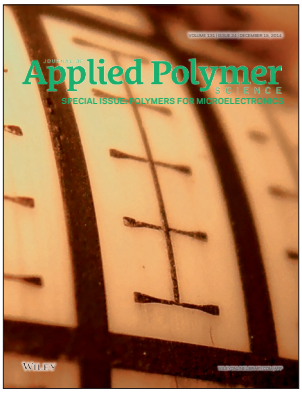

Development of polynorbornene as a structural material for microfluidics and flexible BioMEMS
A. E. Hess-Dunning, R. L. Smith, and C. A. Zorman, *J. Appl. Polym. Sci.* 2014, **DOI:** 10.1002/app.40969

A thin film encapsulation layer fabricated via initiated chemical vapor deposition and atomic layer deposition
B. J. Kim, D. H. Kim, S. Y. Kang, S. D. Ahn, and S. G. Im, *J. Appl. Polym. Sci.* 2014, **DOI:** 10.1002/app.40974

Surface relief gratings induced by pulsed laser irradiation in low glass-transition temperature azopolysiloxanes
V. Damian, E. Resmerita, I. Stoica, C. Ibanescu, L. Sacarescu, L. Rocha, and N. Hurduc, *J. Appl. Polym. Sci.* 2014, **DOI:** 10.1002/app.41015

Polymer-based route to ferroelectric lead strontium titanate thin films
M. Benkler, J. Hobmaier, U. Gleißner, A. Medesi, D. Hertkorn, and T. Hanemann, *J. Appl. Polym. Sci.* 2014, **DOI:** 10.1002/app.40901

The influence of dispersants that contain polyethylene oxide groups on the electrical resistivity of silver paste
T. H. Chiang, Y.-F. Chen, Y. C. Lin, and E. Y. Chen, *J. Appl. Polym. Sci.* 2014, **DOI:** 10.1002/app.41183

Quantitative investigation of the adhesion strength between an SU-8 photoresist and a metal substrate by scratch tests
X. Zhang, L. Du, and M. Zhao, *J. Appl. Polym. Sci.* 2014, **DOI:** 10.1002/app.41108

Thermodynamic and kinetic aspects of defectivity in directed self-assembly of cylinder-forming diblock copolymers in laterally confining thin channels
B. Kim, N. Laachi, K. T. Delaney, M. Carilli, E. J. Kramer, and G. H. Fredrickson, *J. Appl. Polym. Sci.* 2014, **DOI:** 10.1002/app.40790

Journal of Applied Polymer Science

Development of Polynorbornene as a Structural Material for Microfluidics and Flexible BioMEMS

Allison E. Hess-Dunning,[1] Russell L. Smith,[2] Christian A. Zorman[1,2]

[1]Rehabilitation Research and Development, Advanced Platform Technology Center of Excellence, Louis Stokes Cleveland VA Medical Center, Cleveland, Ohio 44106

[2]Department of Electrical Engineering and Computer Science, Case Western Reserve University, Cleveland, Ohio 44016

Correspondence to: C. A. Zorman (E-mail: caz@case.edu)

ABSTRACT: Polynorbornene is a class of polymer that exhibits significant potential as a structural material in microelectromechanical systems owing to its dielectric constant and compatibility with silicon-based microfabrication processes. A commercially available version of PNB (Avatrel™ 2585P) is particularly attractive for bioMEMS applications because of its low moisture absorption characteristics, photodefinability, and potential biocompatibility. This study furthers the advancement of PNB as an enabling structural material for microfluidics and flexible bioMEMS applications by developing the following key processing techniques: (1) oxygen plasma-based surface modification for bonding PNB layers to glass substrates, and (2) the monolithic fabrication of free-standing, mechanically flexible electrode arrays using silicon wafers as mechanical supports during fabrication. To further develop PNB for flexible, implantable bioMEMS applications, this study also includes an evaluation of: (1) the tensile properties of free standing structures after accelerated lifetime testing in phosphate-buffered saline, and (2) the *in vitro* performance of free-standing, mechanically flexible neural microelectrode array-based neural interfaces. © 2014 Wiley Periodicals, Inc. J. Appl. Polym. Sci. **2014**, *131*, 40969.

KEYWORDS: biomedical applications; mechanical properties; microfluidics; sensors and actuators; surfaces and interfaces

Received 4 March 2014; accepted 9 May 2014

DOI: 10.1002/app.40969

INTRODUCTION

Polymers offer unique material properties for microelectromechanical systems (MEMS) that are not offered by silicon, including mechanical flexibility, a high coefficient of thermal expansion, and surfaces that can be functionalized for a specific application (i.e., biocompatibility). From a processing perspective, properties that are required for MEMS include compatibility with structural and sacrificial materials as well as techniques to create patterned structures. Polyimide,[1–4] parylene,[5–7] PDMS,[8–11] benzocyclobutene (BCB),[12,13] and SU-8[14–16] comprise a short list of polymers that have been successfully used in MEMS. Two of the more common technology areas where polymers have found use in MEMS include microfluidic devices and mechanically flexible microelectrode arrays for biosensing and neural interfacing.

Polynorbornene (PNB) is a polycyclic olefin polymer, of which the many commercial varieties have been used in a range of applications that include optical polymers in flat panel displays and waveguides,[17,18] dielectric encapsulants for electronic packaging, sacrificial materials for MEMS,[19] photoresists, and adhesives. Avatrel™ (Promerus, LLC) is a family of PNB formulations developed specifically for electronic packaging, primarily encapsulation of devices (including MEMS),[20–23] dielectric isolation, and stress compensation. One of the primary applications of Avatrel™ has been as an optical interconnect, capitalizing on an optical transparency of at least 96% (for Avatrel™ 2190P) and a refractive index of 1.5–1.55.[24]

Avatrel™ 2585P is a particular PNB formulation that is both spin-castable and photodefinable, providing for straightforward monolithic microfabrication without the use of special techniques or customized tools. A comparison of material properties of Avatrel™ 2585P with those of more commonly used polymers is presented in Table I.[25] Films of up to ~ 100 μm in thickness can be produced from a single spin-cast layer of the polymer. Avatrel™ 2585P exhibits good adhesion to sputtered metals without the need of an adhesion promoter.[26] Moisture absorption is very low and nearly comparable to parylene. Thermal stability and adhesion to metals, silicon, and silicon dioxide are good. Shrinkage on cure is 0.5% or less, compared to other polymer dielectrics which exhibit shrinkage of up to 50%. Avatrel™ films exhibit low stress because of the low shrinkage on cure and the moderate tensile modulus which compensates for thermal stress effects.

Our previous investigations of PNB for bioMEMS applications have shown Avatrel™ 2585P to exhibit good moisture resistance,[27] and initial biocompatibility testing of Avatrel™ 2585P by our

Table I. Properties of Avatrel™ 2585P as Compared with SU-8, Polyimide and Parylene C

Property	Avatrel 2585P	SU-8[a]	Polyimide[b]	Parylene C[c]
Tensile Strength (MPa)	18	60	392	69
Tensile modulus (MPa)	800	2000	8830	3200
Elongation (%)	32	4.8-6.5	30	200
Glass transition temperature (°C)	280	200–210	-	-
Coefficient of thermal expansion (ppm/K)	180	52	12	35
Dielectric constant	2.42 (1MHz)	3.2 (10 MHz)	3.5 (1 kHz)	3.1 (1 kHz)
Specific resistivity (Ω·cm)	2×10^{15} (1 MHz)	7.8×10^{14}	$>10^{16}$	$>10^{16}$
Dielectric strength (V/cm))	4.1×10^{6}	$>4\times10^{5}$	1.5×10^{5}	2.6×10^{6}
Water absorption (%)	0.07	0.55–0.65	0.8–1.4	0.06

Note: The properties of SU-8, polyimide and parylene-C are from Ref. 25.
[a] MicroChem Corp., Newton, MA, USA, Material Data Sheet SU-8 2000 version 2009 and Material Data Sheet SU-8 3000 version 2009.
[b] UBE Europe GmbH Material Data Sheet UBE U-Varnish-S version 2005.
[c] Parylene Coating Services Inc. Material Data Sheet Parylene version 2009.

group has been promising.[28,29] A study reported by Keesara et al. investigated growth of colorectal cancer cells on Avatrel™ 2585P in comparison to a polycarbonate control sample showed no differences in cell growth after 24 and 48 hours. A further study investigated growth of mouse fibroblast cells on Avatrel™ 2585P in comparison to glass, silicon, and silicon dioxide controls after 1, 3, and 7 days.[27] The percentage of total cells still alive on PNB was found to be slightly lower than on glass but comparable to silicon and silicon dioxide. However, the total number of cells on PNB was significantly lower than on control samples. One explanation suggested by the data is that the hydrophobic nature of PNB inhibits cell adhesion.[28] From a processing perspective, its compatibility with conventional photolithographic patterning techniques and resistance to hydrofluoric acid enables Avatrel™ 2585P to be used as the main structural material in free-standing diamond-on-polymer electrode arrays fabricated by a transfer technique.[30–32] These favorable results motivated our effort to further explore the potential of PNB for bioMEMS by developing some of the basic, widely used fabrication processes for Avatrel™ 2585P that are currently absent from the fabricators toolbox. As bioMEMS devices can be broadly divided into two categories: *in vitro* devices, which are typically based on microfluidics fabricated on rigid substrates; and *in vivo* devices, that benefit from mechanical flexibility, we focused this effort into developing surface treatments for bonding and release processes for free-standing structures.

Though primarily used for encapsulation and optical applications, there are some reports of PNB for microfluidics applications. Initial work focused on the formation of PNB-based microchannels and related structures using thermally decomposable polymer sacrificial layers.[19,33,34] Photolithographically patterned PNB has been incorporated into microfluidic devices using two distinct process routes. White et al. describe its use as a photodefinable sacrificial material for serpentine polyimide microfluidic channels.[35] Sekar et al. describe the use of Avatrel™ for sealing silicon microchannels to provide cooling for 3D integrated circuit designs.[36] The microchannels were formed by first patterning channels into the silicon using a etch process, followed by spin-casting and polishing a thermally decomposable sacrificial material, spin-casting an Avatrel™ overcoat, and finally thermally decomposing the sacrificial material. In this design, Avatrel™ was photopatterned into vias but not lateral channels.

PDMS is a preferred material for microfluidic device structures because of the ease and speed of processing. PDMS, as an elastomeric material, is easy to work with once cured and devices can be sealed conveniently by direct contact bonding to PDMS, glass, or silicon after oxygen plasma surface activation.[37] However, the preferred formulations of PDMS require the use of photolithographically-defined molds to create patterned microstructures. A similar bonding process for PNB would offer a convenient method to create microfluidic channels that exhibit a moisture resistance much greater than PDMS and does not require a molding step for pattern generation. To the best of our knowledge, a PNB bonding process of this type has not previously been reported. In an effort to fill this gap, this work investigates surface modification of Avatrel™ 2585P by oxygen plasma treatment for bonding to glass as a first step to developing a fabrication platform for PNB-based microfluidics.

To the best of our knowledge, other than our previous reports on the diamond-on-polymer devices,[27] all reports on Avatrel™-based devices have utilized the polymer on a rigid substrate. However, its mechanical properties suggest that it may also have potential as the principal structural material in flexible MEMS devices. While polymers like polyimide and parylene have been successfully used as the principal structural material in freestanding, mechanically-flexible microelectrode arrays, the combination of mechanics, ease of patterning, adhesion properties, chemical compatibility, and moisture resistance offered by PNB is unmatched. Owing to this unique combination of properties, PNB was investigated as the main structural material in mechanically flexible microelectrode arrays for neural interfacing.

PNB AS A MATERIAL FOR MICROFLUIDICS

Oxygen Plasma Activation of PNB Surfaces

Oxygen plasma treatment of PNB was investigated to determine the parameters which produce the highest degree of hydrophilic behavior as indicated by the minimum contact angle as

Table II. Prediction Model Report for the Oxygen Plasma Treatment Experiments Conducted in this Study

Parameter	Theta	Total sensitivity	Main effect	Time interaction	Power interaction	Flow interaction
Time	0.0046	0.6414	0.0594	.	0.5587	0.0234
Power	0.0193	0.7331	0.0748		.	0.0996
Flow	0.0102	0.1515	0.0286	0.0234	0.0996	.

The report shows strong sensitivity of contact angle to variations in both power and time and a relatively low sensitivity to flow.

determined by a static sessile drop method. Hydrophobic recovery of PNB was also investigated by making contact angle measurements at spaced intervals following plasma treatment. In competing polymer systems (i.e., PDMS), hydrophilic surfaces are required for successful bonding to convenient substrates such as glass.

A total of 24 samples each consisting of a 50-μm-thick PNB film were prepared for the plasma treatment study. Avatrel™ 2585P was spin cast onto a 100 mm silicon wafer at 800 rpm for 10 s followed by 1000 rpm for 30 s. The wafer was soft-baked on a hot plate for 5 minutes at 120°C, exposed to a UV light source fitted with a 365 nm filter, baked on a hot plate for 4 minutes at 90°C, and cured for one hour at 160°C. Samples were diced into ~15 x 15 mm^2 coupons. All samples were washed for 10 seconds in DI water and dried in compressed air after dicing. Samples were handled under a HEPA-filtered flow hood to prevent contamination by dust.

Oxygen plasma surface treatments were performed using a March Instruments™ PX-250™ oxygen plasma system. For this study, the exposure time ranged from 10 to 240 seconds, the power ranged from 8 to 100 W, and the oxygen flow ranged from 8% to 100% of full scale, corresponding to pressures of ~130 to 920 mTorr. Powers greater than 100 W were not investigated because they approach the powers used for plasma etching of PNB and would risk damage to the surface. Parameter ranges were also selected based on the limitations of the plasma treatment system, a preliminary study on six samples over a wide range of process parameters, and optimal treatment parameters for PDMS and SU-8. Contact angle measurements on each sample were made using a custom-built goniometer outfitted with image processing software for contact angle determination.[38] Deionized water was used as the test liquid and calibration was performed using oxidized silicon and polyimide substrates. The experiment was conducted using a 24-point space-filling Latin hypercube design as generated by JMP 9™ statistical software package. The prediction model report and surface profiler plot of the resulting data are provided in Table II and Figure 1.

The prediction model report shows that the total sensitivity of contact angle to flow is 0.15, indicating that variations in flow have only a small effect on contact angle. Flow does not show significant interaction with power or time. The marginal model indicates that there is a slight decrease in contact angle at high flows. The maximum flow setting of 100%, corresponding to a pressure of 920 mTorr, was selected as the optimal flow setting.

The prediction model report shows that power and time have small main effects (first-order effects) on contact angle. However, total sensitivity is high for both: 73.3% and 64.1%, respectively. Total sensitivity includes second-order effects of other parameters. The report indicates that both time and power have a significant effect on contact angle and that this effect depends on their interaction. It is worth noting that 73.3% of the variation in the data is explained by the relationship to power with secondary effects of time and flow. This provides further support that the model is applicable to this data set. Minimal contact angles occurred at powers of 50 and 100 W and at a time of 150 s. Because contact angles associated with powers of 50 and 100 W were nearly the same, the selection between them was made based on the fact that lower power plasma treatment is more attractive for fabrication processes because there is less risk of damage to the PNB or to other materials in the device. An exposure time of 150 s, a power of 50 W, and a flow of 100% produced the minimal contact angle, which was measured after performing the analysis to be 2.2°. It should be noted that the aforementioned prediction model does not take into account the uncertainty in the contact angle measurement, which for small angle measurements was determined experimentally to be ±0.5° for our goniometer. Therefore the graph in Figure 1 represents trends in the behavior which may not be as pronounced when taking into account measurement uncertainty.

Plasma-treated PDMS is known to return to its nominal, untreated contact angle over a period of several days. To determine whether PNB also undergoes hydrophobic recovery, testing was conducted to compare the contact angles of PNB and PDMS at increasing intervals following plasma treatment. Samples were plasma treated under the same conditions in batch and a fresh sample was used for each data point; samples were not reused once subjected to contact angle measurement. For this particular study, two distinct groups of PNB samples were used. One group was treated at the plasma parameters found to produce the minimum contact angle: 150 s, 50 W, and 100% flow. Another group was treated at a lower power and exposure time to determine whether less vigorous plasma treatment resulted in more rapid hydrophobic recovery. This group was treated at 20 W for 20 s at 100% flow which was expected to result in a contact angle that was higher but still less than 5°. The PDMS group was treated with a standard PDMS bonding recipe successfully used in our lab: 25 W for 25 s at 100% flow. Both PNB groups used samples of 50-μm-thick PNB films on silicon substrates and the PDMS group used 60-μm-thick

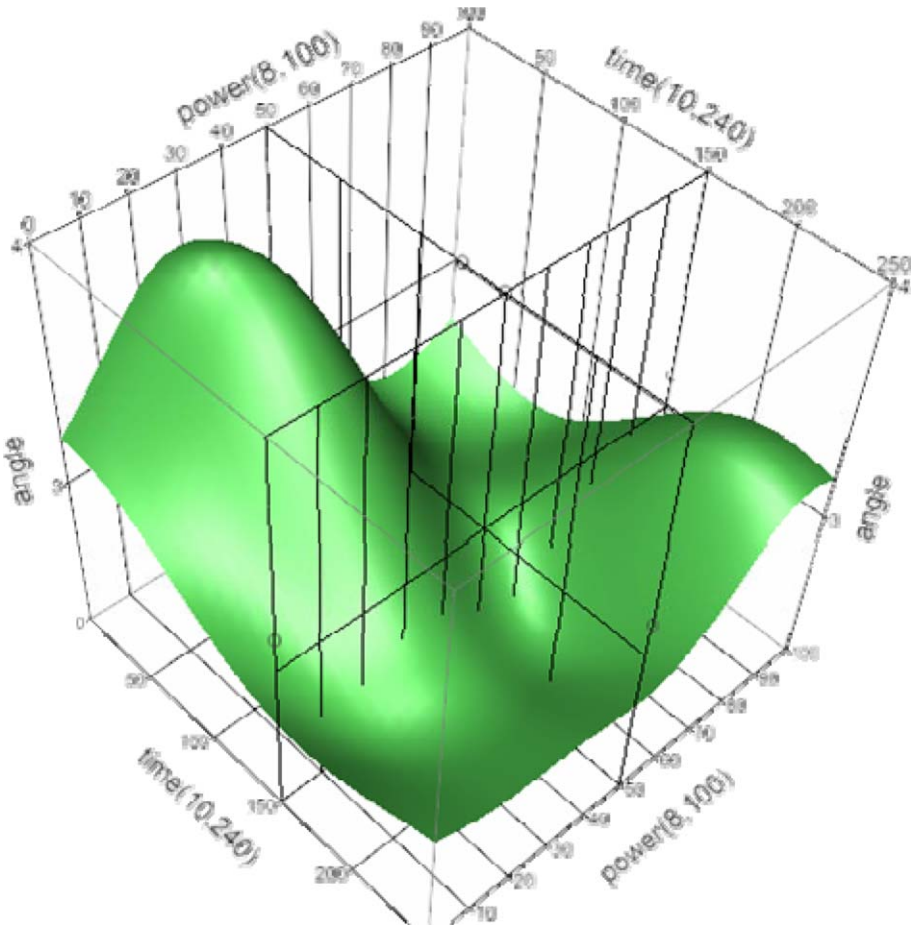

Figure 1. Surface profiler plot for contact angle versus time and power for tests performed using a flow rate of 100%. The intersecting grid (time = 150 s and power = 50 W) is included to indicate the predicted optimal plasma treatment conditions based on the minimum contact angle associated with the surface plot. The experimental data used to generate this plot is tabulated in Ref. 38. [Color figure can be viewed in the online issue, which is available at wileyonlinelibrary.com.]

PDMS films on silicon substrates. Contact angle data is presented in Table III. The largest uncertainties in contact angle measurements were ascribed to variations among repeated measurements and found to be ±1.0° for a surface of angle 76° and ±0.5° for a surface of angle 6.0°. For comparison, the contact angle of untreated PNB was found to be 76° and the contact angle of untreated PDMS was found to be 94°.

Table III. Contact Angle of PNB and PDMS Samples at Increasing Intervals following Plasma Treatment

Time after plasma treatment	PNB at 50 W/150 s/100%	PNB at 20 W/20 s/100%	PDMS at 25 W/25 s/100%
1 min.	2.2°	3.9°	2.1°
5 min.	2.6°	4.2°	2.7°
20 min.	3.1°	4.6°	3.8°
60 min.	2.9°	11.8°	7.5°
3 hour	3.3°	10.1°	12.3°
14 hour	7.7°	13.4°	31.5°
1 day	6.7°	14.2°	50.4°
2 day	6.9°	14.9°	50.5°
4 day	10.1°	17.0°	46.6°

Data shows hydrophobic recovery of PNB occurs more slowly than recovery of PDMS.

As is evident in Table III, hydrophobic recovery of PNB was observed but occurs much more slowly than for PDMS. The PNB treated at the lower power and time setting exhibited a higher contact angle and more rapid recovery than the PNB treated at the higher settings; however, recovery was still slower than the recovery of PDMS.

Experiments were performed to evaluate the bonding of PNB to glass substrates and to determine bond strength for samples treated in oxygen plasma at parameters producing minimum contact angle and at suboptimal treatment parameters. The blister test was selected as a means to evaluate bonding strength because of the ease of sample fabrication, simplicity in execution and direct applicability to microfluidics. For the blister test, a test sample is bonded to a substrate which has an orifice that permits the direct application of force to the bonding interface by pressurization of the bonded structure. Pressure is increased until the bond fails. A schematic of the setup used in this study is shown in Figure 2.

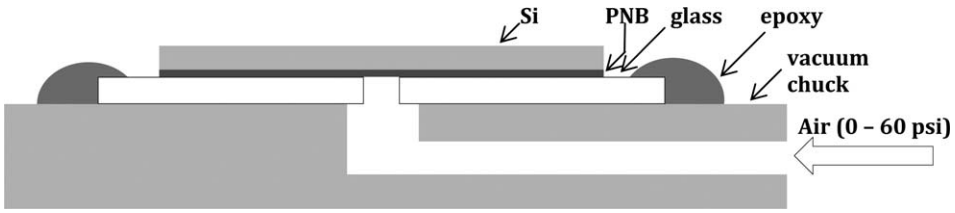

Figure 2. Schematic of the blister test.

Samples consisting of 50-μm-thick PNB films on 15 x 15 mm^2 silicon substrates prepared using the process described previously were used for the bonding study. Fisherfinest™ Premium Cover Glass slides were used as the bonding mates. Prior to bonding, a single ~1.5 mm diameter hole was micromachined into each glass substrate. The 22 x 22 mm^2 glass substrates were cleaned in 2 : 1 v/v 98% H_2SO_4 : 30% H_2O_2 piranha solution for 30 minutes, rinsed with DI water, and dried in compressed air.

The PNB samples were subjected to one of the two oxygen plasma treatments, namely: (1) 50 W for 150 s at 100% flow; or (2) 20 W for 20 s at 100% flow. Bonding was performed by firmly pressing the samples together and heating the bonded pair at 200°C for 30 min. Samples were bonded either immediately after plasma treatment or 60 minutes after plasma treatment. Bonded samples were subjected to applied pressures of up to 60 psi. Results are presented in Table IV. All samples were successfully bonded and no samples failed the pressure test. These results indicate that PNB can be successfully bonded to glass substrates under conditions similar to those used for PDMS and with bond strengths that are comparable to those required of typical microfluidic applications.

PNB AS A MATERIAL FOR MECHANICALLY FLEXIBLE ELECTRODE ARRAYS

Tensile Testing of Free-Standing PNB Structures

To evaluate the effects of a physiological environment on the mechanical properties of PNB, tensile testing was performed on freestanding PNB films that had been immersed in phosphate buffered saline (PBS). This was important to ensure that implantation of a PNB-based device into a biological system would not result in immediate, catastrophic mechanical failure. In this experiment, eight freestanding, macroscale PNB strips with dimensions 10 x 60 mm^2 were prepared by first spin-casting a 50-μm-thick PNB film onto a Si wafer with a 1-μm-thick thermal SiO_2 layer. The film was then soft-baked on a hotplate for 5 minutes at 120°C, and then patterned using i-line UV radiation through a 365 nm filter for 312.5 s, for a total dose of 2 J. The film was postexposure baked for 4 minutes at 90°C, then spray-developed using methyl amyl ketone (MAK) and rinsed with PGMEA. The film was then cured in a polymer curing furnace in a nitrogen environment for 1 hour at 160°C. Next, a 12-μm-thick PNB layer was cast on top of the patterned 50 μm strips on the wafer. The film was then soft-baked on a hotplate for 5 minutes at 120°C, and then patterned using i-line UV radiation through a 365 nm filter for a total dose of 1.6 J. The film was postexposure baked for 4 minutes at 90°C, then spray-developed using MAK and rinsed with PGMEA. The film was then cured in a polymer curing furnace for 1 hour at 160°C. The two-layer PNB test strips were then released from the wafer by dissolving the thermal SiO_2 layer in HF.

Four of the PNB strips were soaked in PBS (pH 7.4) for 72 hours at 87°C to simulate extended exposure to the PBS under operating conditions at physiological temperature (37°C). According to the 10° rule, the acceleration factor doubles for every 10° increase in temperature.[39] Therefore, the acceleration factor for a 50°C increase in temperature can be estimated to be 32. As a result, 3 days at 87°C is expected to be the equivalent of 96 days at 37°C in PBS. At this rate, to find the effects of saline on PNB at body temperature for 20 years, the PNB test strips would need to be soaked for approximately 228 days at 87°C. The remaining four PNB strips were left as-fabricated and stored in a dry box. Each PNB strip was subjected to microtensile testing to failure with an Instron™ 5564 tool.

Table IV. Blister Test Results for Tests Conducted After Bonding

	Oxygen plasma treatment					
Sample	Time (seconds)	Power (W)	Flow (% of max.)	Delay before bonding	Expected contact angle at bonding	Result
1	150	50	100%	Immediate	2.2°	Held to 60 psi
2	150	50	100%	Immediate	2.2°	Held to 60 psi
3	150	50	100%	60 minutes	2.9°	Held to 60 psi
4	150	50	100%	60 minutes	2.9°	Held to 60 psi
5	20	20	100%	Immediate	3.9°	Held to 60 psi
6	20	20	100%	Immediate	3.9°	Held to 60 psi
7	20	20	100%	60 minutes	11.8°	Held to 60 psi
8	20	20	100%	60 minutes	11.8°	Held to 60 psi

All samples held to 60 psi.

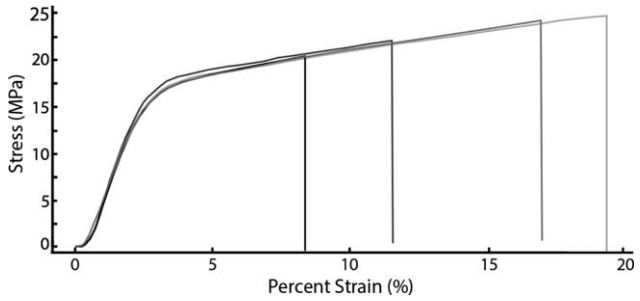

Figure 3. Stress vs. strain curves for each of the four as-fabricated (no soaked) PNB strips.

Representative stress–strain plots of macro-scale samples are shown in Figures 3 and 4, and tensile testing data are summarized in Table V. The mechanical properties of the as-fabricated PNB strips match well with literature values of Avatrel™ 2585P. After soaking in PBS for 72 hours, there was a 16% reduction in Young's modulus ($P = 0.00235$, t-test). This increase in flexibility may be desirable because it reduces the mechanical mismatch between the microfabricated electrode structure and the nerve tissue, which has a Young's modulus on the order of 1–100 kPa.[40] Based on a t-test analysis of the data, there were no statistically significant differences in strain-to-break ($P = 0.25$, t-test) or tensile strength ($P = 0.52$, t-test) between the as-fabricated and soaked samples. However, the soaked samples had a much less variability in strain-to-break, with three of the four samples having a strain-to-break of at least 18%. In comparison, three of the four as-fabricated samples had a strain-to-break of less than 18%. Under accelerated testing equivalent to 32 days under physiological conditions, the mechanical properties after soaking in PBS remain stable.

To evaluate the tensile properties of PNB translate to microscale dimensions, freestanding, microfabricated structures (Figure 5) were also subjected to mechanical testing using a custom microtensile tester that has been documented previously.[41,42] Each 50-µm-thick dogbone-shaped test structure comprised a 275 µm-wide x 2 mm-long beam with 2 mm x 1.5 mm pads on either end to facilitate gripping. The structures were fabricated by spin-casting a 50-µm-thick PNB layer onto an Si wafer with a 1-µm-thick thermal SiO_2 layer using the same parameters described for the 50-µm-thick layer of the larger tensile structures. The samples were released by immersing the wafer in 49% HF to dissolve the SiO_2 film.

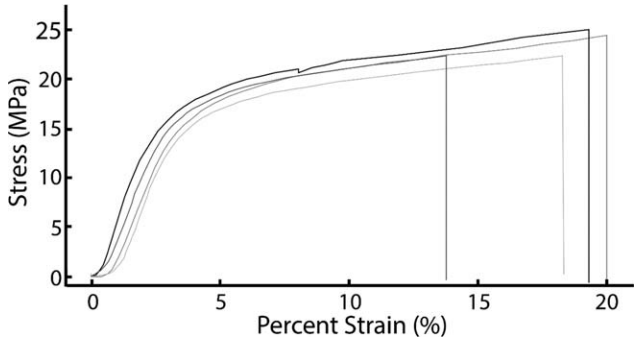

Figure 4. Stress vs. strain curves for each of the four PNB strips subjected to accelerated testing in PBS.

Table V. Comparison of Young's Modulus, Percent Strain at Break, and Tensile Strength of Unsoaked PNB Strips and PNB Strips Soaked in PBS for 72 hours at 87°C

Sample type	Young's modulus (MPa)	Strain-to-break (%)	Tensile strength (MPa)
Unsoaked	887 ± 26	13.6 ± 5.0	22.6 ± 1.9
Soaked	742 ± 51	17.2 ± 2.7	23.5 ± 1.5

The mechanical properties of microscale PNB structures, as measured using a microtensile tester,[45,46] are summarized in Table VI. Young's modulus and the percent strain-to-break are comparable to the macroscale samples. The tensile strength of the microscale samples was greater than that of the much larger macroscale samples. Reducing the sample volume by 99.9% would reduce the probability of a flaw in the sample, yielding the higher tensile strengths observed for the microfabricated PNB devices.[43]

While the macroscale sample dimensions are relevant for peripheral nerve interfaces or cortical surface neural interfaces, the microscale dimensions are relevant for use in penetrating biosensors, such as intracortical probes. The microscale mechanical characterization suggests that the bulk mechanical properties scale to microscale dimensions.

Fabrication of Free-Standing Microelectrode Arrays

Functional, free-standing PNB-based devices were fabricated using photolithography-based processes. Two different processes were used to produce PNB-based microelectrode arrays for neural interfacing (Figure 6). The primary differences between the two processes are the sacrificial layers onto which the PNB films are cast and processed, and the method of dissolving the sacrificial release layer. One process utilized a Si wafer with a 1-µm-thick thermal SiO_2 surface film as the handle wafer onto which the PNB-based devices were built (Figure 6, step 1a). For the second process, the PNB-based devices were built on Si wafers coated with sputter-deposited 100 nm Cr and 500 nm Al layers (Figure 6, step 1b).

Steps 2, 3, and 4 were identical for both processes. A 50-µm-thick PNB film was spin-cast onto the wafer, patterned, and processed in the same manner as the corresponding film for the tensile testing strips described above (Figure 6, step 2). Next, the PNB surface was prepared for metal deposition and patterning (Figure 6, step 3) by spin-casting and patterning AZ™

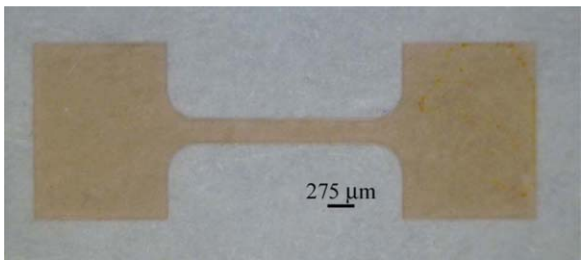

Figure 5. Microscale PNB tensile testing sample. [Color figure can be viewed in the online issue, which is available at wileyonlinelibrary.com.]

Table VI. Mechanical Properties of as-Fabricated Microscale PNB Samples as Measured by Microtensile Testing

Sample type	Young's modulus (MPa)	Strain-to-break (%)	Tensile strength (MPa)
Microscale	848 ± 65	19.5 ± 13.2	65 ± 16

nLOF 2035 negative tone photoresist on the PNB base layer. The photoresist was processed according to product documentation, immersion-developed for 120 s in AZ™ MIF 300, then rinsed in deionized water and dried using a nitrogen gun. Thin film metal electrode contacts, interconnect traces, and contact pads were sputter-deposited. To promote metal adhesion to the PNB surface, the wafer was subjected to an Ar plasma-based RF preclean for 90 s at 125 W in the sputter system under vacuum. Next, either a 30 nm Cr adhesion layer and 250 nm Pt conductor layer (SiO_2 sacrificial layer) or a 20 nm Ti adhesion layer and 250 nm Pt conductor layer (Al sacrificial layer) were sputter-deposited under vacuum on the PNB base layer and negative-tone resist. The metal patterning was completed in a liftoff step with the aid of ultrasonic agitation in the solvent AZ™ EBR 70/30. The wafer was then rinsed with DI water. Finally, a 12-μm-thick PNB capping layer was deposited and processed using the same process used for the 12-μm-thick PNB layer used for the PNB tensile testing strips, described above (Figure 6, step 4).

After patterning of the PNB capping layer was complete, all device layers had been deposited and patterned. The final step in device fabrication was to release the devices from the wafer. Devices built on a thermal SiO_2 film were released by dissolving the SiO_2 in 49% HF for approximately 3 hours (Figure 6, step 5a). Devices built on a Cr/Al film were released by anodic aluminum dissolution.[44] The wafer was immersed in 2 L of 2*M* NaCl in DI water. A power supply was connected to both the wafer and a piece of stainless steel foil with alligator clips, and both the wafer and foil were submerged in the solution. The potential between the foil and the wafer was set to 0.70 V. As the Al dissolved, the Cr layer remained intact, providing a continuous conductive film across the wafer. After approximately 2 hours, the structures fully released from the wafer and floated to the top of the salt water solution.

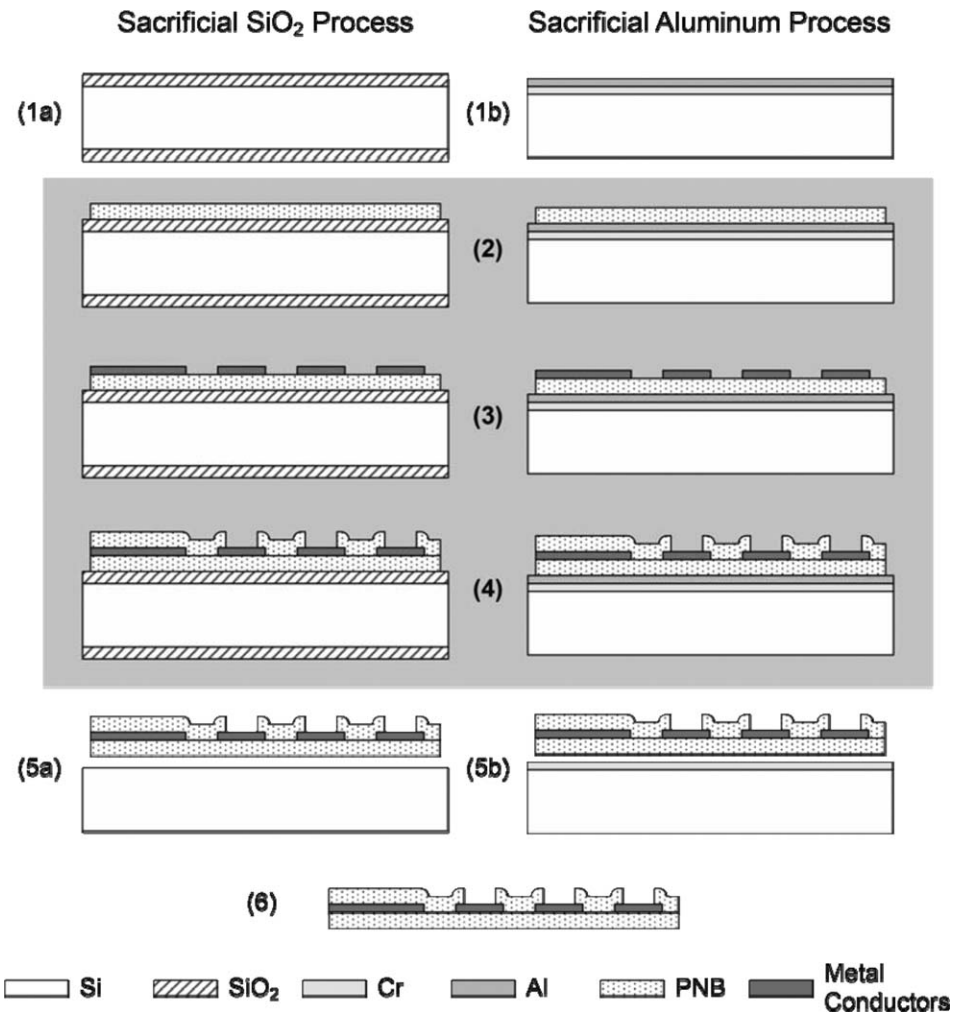

Figure 6. Process sequence for fabricating PNB-based electrode structures with either an HF-based SiO_2 dissolution release or an anodic aluminum release. The steps within the shaded area indicate steps that are identical for both the sacrificial SiO_2 process and the sacrificial aluminum process.

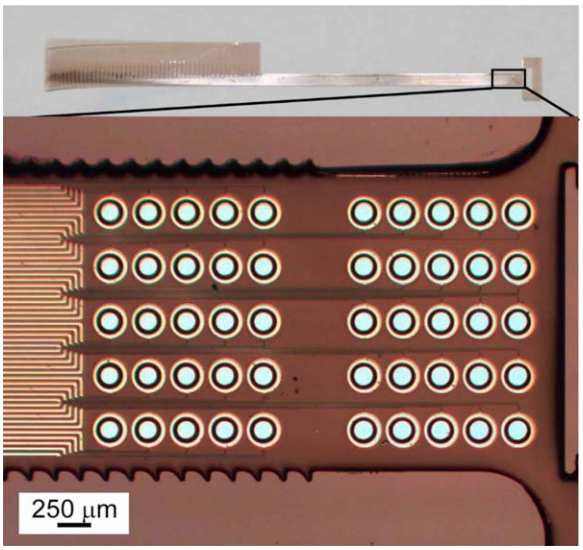

Figure 7. Released PNB electrode array with Cr/Pt metallization: (top) global view of the device showing the connector region on the left and bio-interface region on the right; and (bottom) magnified view of the bio-interface region showing the array of 50 microelectrodes. [Color figure can be viewed in the online issue, which is available at wileyonlinelibrary.com.]

Freestanding, metallized PNB-based electrode arrays were successfully fabricated, as shown in Figure 7. Features as small as 50 μm were resolved in the 50-μm-thick PNB film, for an aspect ratio of ~1 : 1. PNB retained its structural integrity even after exposure to organic solvent-based photoresist, tetra-methyl ammonium hydroxide (TMAH)-based photoresist developer (2 minutes), propylene glycol methyl ether (PGME)/propylene glycol monomethyl ether acetate (PGMEA)-based photoresist solvent for liftoff (~8 hours), and the release process (~6 hours). Two release processes were presented: one based on a SiO_2 sacrificial film, and one based upon a sputtered Al sacrificial film. The advantages of the sacrificial SiO_2-based process include the batch preparation of Si/SiO_2 wafers, allowing them to be purchased at relatively low cost. However, this process requires HF to dissolve the sacrificial oxide film. Aside from the toxicity of HF, it is incompatible with various materials, including the commonly used Ti adhesion layer. The sacrificial Al-based process requires that each wafer be prepared at higher cost or only one or two at a time. However, the solvent is simply a salt water solution and is compatible with most materials during the time course of the anodic Al dissolution process. As a result, the sacrificial layer and release process chosen should be dependent upon chemical compatibilities with the other materials in the device, as well as available resources.

The functionality of the 50-contact, PNB-based neural electrode arrays were evaluated on the benchtop by measuring the electrochemical impedance in PBS (pH 7.4) of each electrode versus platinum mesh electrode at a frequency of 1 kHz. Typical impedance values of the electrodes on the PNB-based arrays at a frequency of 1 kHz were 25–90 kΩ, with a phase angle of 75°. This indicated that the PNB capping layer was completely removed from the electrode surface during the final development step. Complete exposure of the Pt surface at the electrode is necessary for interfacing with biological systems.

Functionality in biological systems was assessed using a highly studied and well-known invertebrate neural system, the buccal ganglion, and nerves from *Aplysia californica*. The *Aplysia* buccal ganglion and associated nerves were dissected from the anesthetized animal, and placed in a dish and immersed in *Aplysia* saline.[45,46] The PNB-based structure was pressed against a dissected *Aplysia* buccal ganglion using a glass suction electrode [Figure 8(a)]. A suction electrode was used to record from one of the buccal nerves (BN2).[46] Spontaneous neural signals from the nerve and the ganglion were simultaneously recorded using an ac-coupled differential amplifier and bandpass filtered (300–1000 Hz).

A battery of tests was performed using the buccal ganglion to determine the effectiveness of PNB-based neural electrode arrays. Figure 8(b) shows the simultaneous recording of spontaneous neural activity through a standard nerve suction electrode and an electrode on the microfabricated PNB electrode array. The peak-to-peak noise level and signal amplitude of the nerve electrode and PNB array electrode recordings are comparable at ~7 and 30 μV, respectively. The close correspondence between the timing of the two recordings indicates that the microfabricated electrode is making viable contact to the nerve. Some spikes appear on the nerve recording and not on the PNB array electrode recording, indicating that there is no significant crosstalk between the array recording and the conventional recording. This recording indicated that the PNB-based device was functional and capable of recording neural activity in a

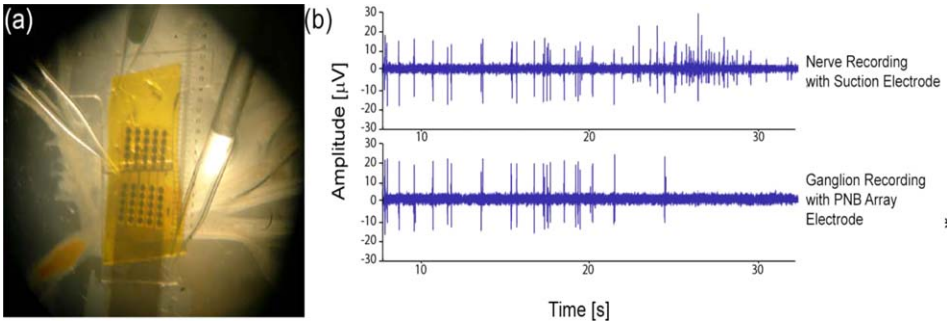

Figure 8. (a) 50-electrode PNB-based array pressed on a dissected *Aplysia* buccal ganglion; (b) Comparison of array electrode recording to a standard nerve suction electrode. [Color figure can be viewed in the online issue, which is available at wileyonlinelibrary.com.]

physiological environment. Recordings from two adjacent electrodes on the same array interfacing with the buccal ganglion had spikes recorded on both electrodes, and the spikes on the two electrodes occurred at different times. This indicated that there was no cross-talk between the two electrodes on the array. This functionality indicates that for acute experiments, the seal between the base and capping PNB layers was sufficient for preventing moisture permeation between adjacent traces.

CONCLUSIONS

The findings described in this study suggest that PNB has the potential to be a highly versatile structural material for bio-MEMS. With regards to oxygen plasma-based surface modification, PNB compares favorably to PDMS with respect to the level of hydrophilicity initially achieved, but significantly outperforms PDMS in the stability of the modified surfaces over time. Such stability has potential impact in microfluidics where stable hydrophilic surfaces aid in device assembly as well as diffusion driven flow. With regards to the mechanical properties after accelerated lifetime testing in phosphate-buffered saline designed to simulate a 3 month deployment, PNB exhibits about a 15% decrease in Young's modulus, while strain-to-break and tensile strength remain stable, which are all compatible with implantable microelectrode arrays for long-term applications. A photodefinable version of PNB (Avatrel™ 2585P) is chemically compatible with SiO_2 and Al-based sacrificial etch processes, enabling the monolithic fabrication of large-area, highly flexible, free-standing microelectrode arrays that have been successfully used to record neural signals from an invertebrate animal model without cross-talk between channels while in solution.

ACKNOWLEDGMENTS

The authors would like to acknowledge Promerus, LLC for providing the Avatrel™ solutions, Mr. Jeremy Dunning for help in microfabrication and benchtop testing, Maria D'Agostino for developing the goniometer and Prof. Hillel Chiel and Hui Lu for assistance on in vitro testing of the electrode arrays. The authors also acknowledge the Advanced Platform Technology Center at the Louis Stokes Cleveland VA Medical Center and the Case Alumni Association for financial support of this research.

REFERENCES

1. Meitl, M. A; Zhou, Y.; Gaur, A.; Jeon, S.; Usrey, M.; Strano, M. S.; Rogers, J. A. *Nano Lett.* **2004**, *4*, 1643.
2. Jeon, M.; Cho, J.; Kim, Y. K.; Jung, D.; Yoon, E. -S.; Shin, S.; Cho, I-J. *J. Micromech. Microeng.* **2014**, *24*, 025010.
3. Gonenli, I. E.; Celik-Butler, Z.; Butler, D. P. *J. Microelectromech. Syst.* **2011**, *11*, 2318
4. Metz, S.; Holzer, R.; Renaud, P. *Lab Chip* **2001**, *1*, 29.
5. Ziegler, D.; Suzuki, T.; Takeuchi, S. *J. Microelectromech. Syst.* **2006**, *15*, 1477.
6. Gensler, H. M.; Meng, E. *J. Micromech. Microeng.* **2012**, *22*, 115031.
7. Gensler, H.; Sheybani, R.; Li, P. -Y.; Mann, R. L. O.; Meng, E. *Biomed. Microdevices* **2012**, *14*, 483.
8. Schneider, F.; Draheim, J.; Kamberger, R.; Wallrabe, U. *Sens. Actuators A Phys.* **2009**, *151*, 95.
9. Mannsfeld, S. C. B.; Tee, B. C. -K.; Stoltenberg, R. M.; Chen, C. V. H. -H.; Barman, S.; Muir, B. V. O.; Sokolov, A. N.; Reese, C.; Bao, Z. *Nat. Mater.* **2010**, *9*, 859.
10. Fiddes, L. K.; Raz, N.; Srigunapalan, S.; Tumarkan, E.; Simmons, C A.; Wheeler, A. R.; Kumacheva, E. *Biomaterials* **2010**, *31*, 3459.
11. Hosokawa, K.; Hanada, K.; Maeda, R. *J. Micromech. Microeng.* **2002**, *12*, 1.
12. Zhou, X.; Virasawmy, S.; Quan, C. *Microsyst. Technol.* **2008**, *15*, 573.
13. Lee, K.; He, J.; Clement, R.; Massia, S.; Kim, B. *Biosens. Bioelectron.* **2004**, *20*, 404.
14. Hopcroft, M.; Kramer, T.; Kim, G.; Takashima, K.; Higo, Y.; Moore, D.; Brugger, J. *Fatigue Fract. Eng. Mater. Struct.* **2005**, *28*, 735.
15. Lorenz, H.; Despont, M.; Fahrni, N.; LaBianca, N.; Renaud, P.; Vettiger, P. *J. Micromech. Microeng.* **1997**, *7*, 121.
16. Fernández, L. J.; Altuna, A.; Tijero, M.; Gabriel, G.; Villa, R.; Rodríguez, M. J.; Batlle, M.; Vilares, R.; Berganzo, J.; Blanco, F. J. *J. Micromech. Microeng.* **2009**, *19*, 25007.
17. Fujiwara, M.; Shirato, Y.; Owari, H.; Watanabe, K.; Matsuyama, M.; Takahama, K.; Mori, T.; Miyao, K.; Choki, K.; Fukushima, T.; Tanaka, T.; Koyanagi, M. *Jpn. J. Appl. Phys.* **2007**, *46*, 2395.
18. Glukh, K.; Lipian, J. -H.; Mimna, R.; Neal, P. S.; Ravikiran, R.; Rhodes, L. F.; Shick, R. A.; Zhao, X. -M. *Proc. SPIE* **2000**, *4106*, 43.
19. Joseph, P. J.; Kelleher, H. A.; Allen, S. A. B.; Kohl, P. A. *J. Micromech. Microeng.* **2005**, *15*, 35.
20. Monajemi, P.; Joseph, P. J.; Kohl, P. A.; Ayazi, F. *Proc. IEEE Adv. Packag. Mater. (APM)* **2006**, 139.
21. Shick, R. A.; Jayaraman, S. K.; Goodall, B. L.; Rhodes, L. F.; McDougall, W. C.; Kohl, P.; Bidstrup-Allen, S. A.; Chiniwalla, P. *Adv. Microelectron.* **1998**, *25*, 13.
22. Rais-Zadeh, M.; Member, S.; Kohl, P. A.; Ayazi, F.*J. Microelectromechanical Syst.* **2008**, *17*, 78.
23. Joseph, P. J.; Monajemi, P.; Ayazi, F.; Member, S.; Kohl, P. A. *IEEE Trans. Adv. Packag.* **2007**, *30*, 19.
24. Bakir, M. S.; Kohl, P. A.; Glebov, A. L.; Elce, E.; Bhusari, D.; Lee, M. G.; Meindl, J. D. Flexible Polymer Pillars for Optical Chip Assembly: Materials, Structures, and Characterization. In: Earman, A. M.; Chen, R. T.; Eds. Integr. Optoelectron. Devices 2007, International Society for Optics and Photonics; **2007**, p 647802.
25. Hassler, C.; Boretius, T.; Steiglitz, T. Polymers for Neural Implants. *J. Polym. Sci. B Polym. Phys.* **2011**, *49*, 18.
26. Grove, R.; Kohl, P. A.; Shick, R. A.; Goodall, B. L.; Group, A. T. Properties and Processing of AVATREL™ as a High Performance Dielectric. Multichip Modul. 1997. Int. Conf. Denver, CO, **1997**; p 224.

27. Hess, A. E.; Dunning, J. L.; Tyler, D. J.; Zorman, C. A. *Transducers IEEE* **2007**, 1235.

28. Hess, A. E.; Dunning, J.; Tyler, D.; Zorman, C. A. Development of a Microfabricated Flat Interface Nerve Electrode Based on Liquid Crystal Polymer and Polynorbornene Multilayered Structures. Neural Eng. 2007. CNE '07. 3rd Int. IEEE/EMBS Conf., Kohala Coast, HI, **2007**; p 32.

29. Keesara, V. V.; Durand, D. M.; Zorman, C. A. Fabrication and Characterization of Flexible.; Microfabricated Neural Electrode Arrays Made from Liquid Crystal Polymer and Polynorbornene. *MRS Proc* **2006**, *926*, 0926–CC06–04.

30. Hess, A.; Sabens, D. M.; Martin, H. B.; Zorman, C. A. Polycrystalline Diamond-on-Polymer Microelectrode Arrays for Mechanically-Flexible Neural Interfacing. Hilt Head Work 2010 A Solid-State Sensors, Actuators Microsystems Workshop, **2010**.

31. Hess, A. E.; Sabens, D. M.; Martin, H. B.; Zorman, C. A. *J. Microelectromech. Syst.* **2011**, *20*, 867.

32. Hess, A. E.; Sabens, D. M.; Martin, H. B.; Zorman, C. A. *Electrochem. Solid State Lett.* **2010**, *13*, J129.

33. Reed, H. A.; White, C. E.; Rao, V.; Allen, S. A. B.; Henderson, C. L.; Kohl, P. A. *J. Micromech. Microeng.* **2001**, *11*, 733.

34. King, C. R.; Sekar, D.; Bakir, M. S.; Dang, B.; Pikarsky, J.; Meindl, J.D. 3D stacking of chips with electrical and microfluidic I/O interconnects. 2008 58th Electron Components Technol Conference, **2008**, 1.

35. White, C. E.; Anderson, T.; Henderson, C. L.; Rowland, H. D.; King, W. P. *Proc. SPIE Emerg. Lithogr. Technol. VIII* **2004**, *5374*, 361.

36. Sekar, D.; King, C.; Dang, B.; Spencer, T.; Thacker, H.; Joseph, P.; Bakir, M.; Meindl, J. 2008 Int. Interconnect. Technol. Conf. **2008**, *13*.

37. Duffy, D. C.; McDonald, J. C.; Schueller, O. J.; *Anal. Chem.* **1998**, *70*, 4974.

38. Smith, R. L. Oxygen Plasma Surface Activation Of Polynorbornene For Bonding To Glass With Applications To Microfluidic Systems. MS Thesis, Case Western Reserve University, Cleveland, Ohio USA, May **2011**.

39. Hukins, D. W. L.; Mahomed, A.; Kukureka, S. N. *Med. Eng. Phys.* **2008**, *30*, 1270.

40. Borschel, G. H.; Kia, K. F.; Kuzon, W. M. *J. Surg. Res.* **2003**, *114*, 133.

41. Hess, A. E.; Capadona, J. R.; Shanmuganathan, K.; Hsu, L.; Rowan, S. J.; Weder, C.; Tyler, D. J.; Zorman, C. A. *J. Micromech. Microeng.* **2011**, *21*, 54009.

42. Hess, A. E.; Potter, K. A.; Tyler, D. J.; Zorman, C. A.; Jeffrey, R. C. *J. Vis. Exp.* **2013**, *78*, doi: 10.3791/50078.

43. Hemker, K. J.; Sharpe, W. N. *Annu. Rev. Mater. Res.* **2007**, *37*, 93.

44. Metz, S.; Bertsch, A.; Renaud, P. *J. Microelectromech. Syst.* **2005**, *14*, 383.

45. Halpern, J. M.; Xie, S.; Sutton, G. P.; Higashikubo, B. T.; Chestek, C. A.; Lu, H.; Chiel, H. J.; Martin, H. B. *Diam. Relat. Mater.* **2006**, *15*, 183.

46. Lu, H.; Chestek, C. A.; Shaw, K. M.; Chiel, H. J. *J. Neural Eng.* **2008**, *5*, 287.